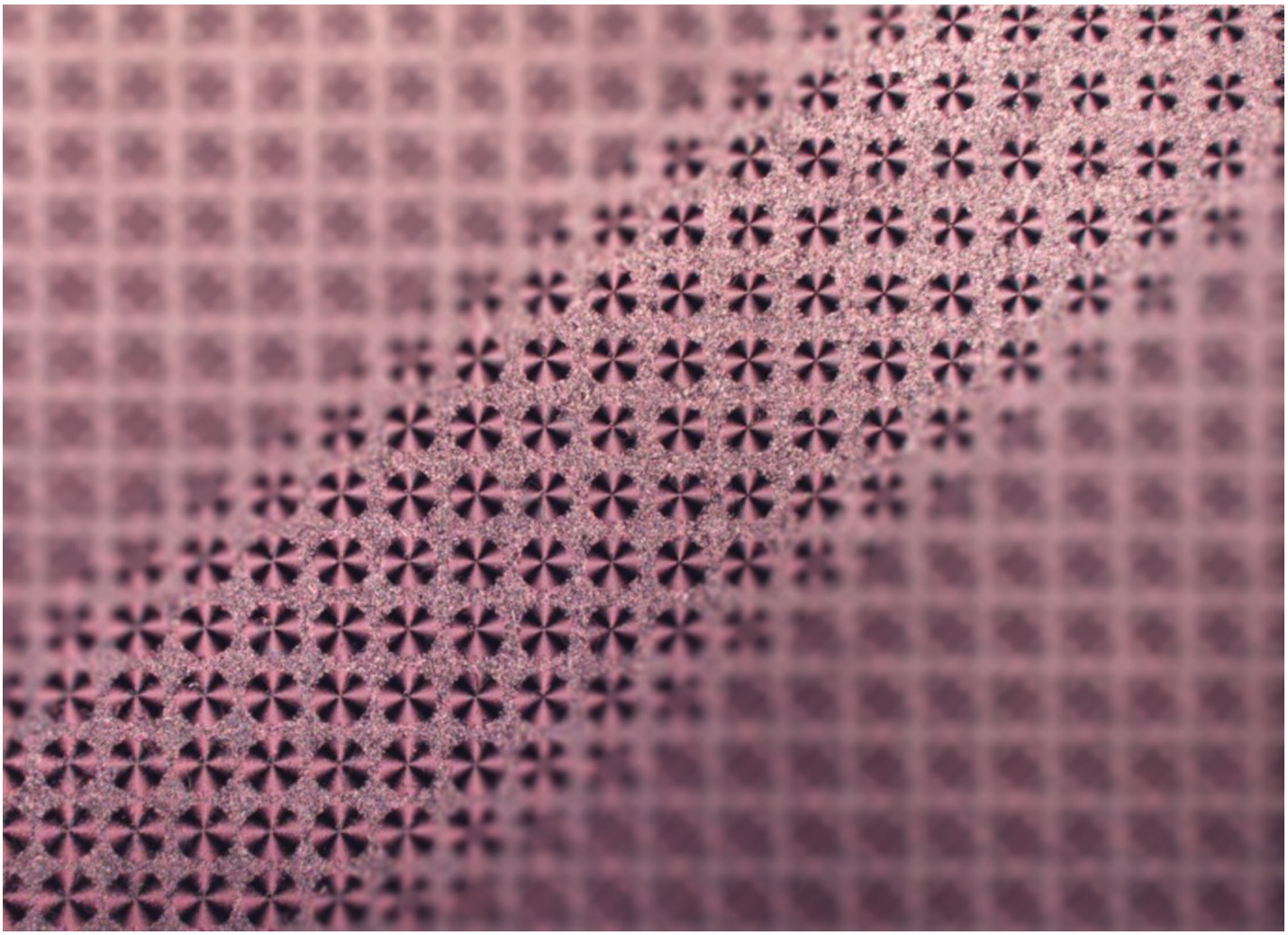

Highlighting Research from the Air Force Research Laboratory from the group of Dr Timothy J. White.

Voxel resolution in the directed self-assembly of liquid crystal polymer networks and elastomers

The directed self-assembly of liquid crystalline materials *via* light-directed surface alignment can yield polymeric materials retaining complex and arbitrary director profiles. Kowalski *et al*. detail theory-backed experimental results to bound the resolution limits of this method to localizing the director within a volume element (voxel).

As featured in:

See Timothy J. White *et al*., *Soft Matter*, 2017, **13**, 4335.

ROYAL SOCIETY OF CHEMISTRY

rsc.li/soft-matter-journal

Registered charity number: 207890

Soft Matter

PAPER

View Article Online
View Journal | View Issue

Cite this: *Soft Matter*, 2017, 13, 4335

Voxel resolution in the directed self-assembly of liquid crystal polymer networks and elastomers

Benjamin A. Kowalski,† Vincent P. Tondiglia,† Tyler Guin† and Timothy J. White *

Received 3rd April 2017,
Accepted 16th May 2017

DOI: 10.1039/c7sm00663b

rsc.li/soft-matter-journal

Monomeric mixtures formulated to prepare a liquid crystal polymer network (LCN) or elastomer (LCE) can be "programmed" by surface alignment to retain complex and arbitrary spatial distributions of the director orientation upon polymerization. The localized control of orientation in a given volume (voxel) within these materials is the subject of intense research, currently motivated by the prospect of distinctive mechanical responses (both active and passive). Here, we report on a rapid and scalable photopatterning method to prepare alignment surfaces with a throughput of 10 mm^2 s^{-1}, using a commercial spatial light modulator and projection optics. Enabled by this method, we detail that the resolution limit of the inscribed director profile is not dictated by the optical system but is determined by the elastic-mediated orientational relaxation of the liquid crystalline materials. A simple model is experimentally validated and the implications for device design are discussed.

Introduction

Liquid crystal networks and elastomers (LCNs, LCEs) are promising stimuli-responsive materials. The mechanical response of these anisotropic materials can reach directional strains of as much as 400%. Localization of the mechanical response in these materials through arbitrary, spatial control of the orientation of liquid crystallinity has opened up new avenues to producing complex and reversible shape change[1] and novel geometric-phase optical elements.[2] Patterning techniques that are modular, scalable (large or small), and rapid (high throughput) will further enable the fundamental exploration of these materials and necessary for translation of this understanding into end use applications.

Foundational research of these materials has focused on macroscopic alignment *via* mechanical stretch (the Finkelmann method),[3] mechanical shear, uniform applied magnetic field[4] or alignment surfaces.[5] An initial effort details localizing the alignment of these materials by simply scribed alignment materials with a profilometer probe tip.[6] Photoalignment of command surfaces composed of photochromic dye molecules has become an appealing approach to directing the local orientation of these materials as it is non-contact, high-resolution, rapid, and scalable.[7] Photoalignment of azobenzene or other dye molecules occurs upon exposure to linearly polarized light which directs the alignment of the molecules in the command surface through either orientationally selective photo-isomerization, photo-crosslinking (LPP), photo-degradation (reviewed in ref. 7 and 8), or reorientation through sequential isomerization events.

Directing the self-assembly of the mesogenic constituents of the monomeric mixture to ultimately result in the synthesis of liquid crystal networks and elastomers with arbitrarily complex topologies necessitates optical methods that afford fine spatial control of the location and polarization of irradiation. Initial research employed sequential mask exposures with successive adjustment to the alignment of the linear polarization of the irradiating source.[9] Subsequently, more complex and specialized exposure schemes have been developed for specific patterns such as turntable methods to produce radial patterns[10] and the use of interference holography to yield small-pitch periodic patterns.[11] Other optical schemes are flexible enough to generate fully arbitrary polarization profiles. For example, a plasmonic mask can transmit locally modulated polarization in a single exposure, based on the local orientation of subwavelength apertures.[12] However, this approach is not reconfigurable, and the fabrication of new masks *via* focused-ion-beam (FIB) etching is a tedious and fundamentally serial process. In the patterning scheme described in ref. 13, a focused laser beam is rastered across a surface while its polarization is modulated to realize fully arbitrary profiles. The throughput of this patterning process is dependent on the profile, but 30 min cm^{-2} is reported. The focused spot size in this scheme can be substantially reduced[14] but this significantly affects the throughput of the method. Similar tradeoffs apply to step-by-step direct-write optical

Air Force Research Laboratory, Materials and Manufacturing Directorate, Wright-Patterson Air Force Base, Ohio 45433-7750, USA.
E-mail: Timothy.White.24@us.af.mil; Tel: +1-937-255-9551
† Also with Azimuth Corporation, 4027 Colonel Glenn Hwy, Beavercreek, Ohio 45431, USA.

lithography that has been employed to inscribe microgrooves in a photoresist.[15]

The optical approaches discussed hereto are serial processes. Large gains in throughput, fidelity, reproducibility, and scalability can be realized by developing and employing parallel exposure methods. Towards this end, here we report on a simple optical scheme, adapted from the holographic recording literature.[16] We employ a commercial spatial light modulator (twisted nematic orientation, TN-SLM) to image onto the target so that the polarization states of each of the $\sim 10^6$ pixels can be independently modulated in a single exposure. This system is easily fabricated (and reproduced) and the polarization pattern is reconfigurable at display rates. We estimate that this system is capable of throughput of nearly 10 $mm^2\ s^{-1}$, an improvement of nearly two orders of magnitude over previous work. At the patterning resolutions achievable with this system, orientational relaxation effects within the volume of the cell are non-negligible. This imposes a fundamental limit on voxel resolution within LCE and LCN, regardless of patterning technique. We analyze this using a simplified expression for Frank elastic energy penalties and find reasonably good agreement with measurements.

Results and discussion

The optical design is shown in schematic form in Fig. 1(a). The 445 nm laser diode beam is s-polarized, spatially filtered, collimated, and apodized, before being transmitted through the spatial light modulator (SLM). An inexpensive, commercially available SLM is used (HoloEye LC-2002; twisted nematic (TN) mode). It consists of a display-resolution array of pixels (800 × 600), each of which is independently addressed by a grayscale signal of 8-bit depth determining the applied electric field, and thus the amount by which the incident linear polarization is rotated. Thus, the transmitted light has spatially patterned polarization angle but uniform intensity (since no analyzer is placed behind the SLM).

Subsequently, a 4f lens relay images the SLM onto the target. This configuration provides easy access to the Fourier plane, where an amplitude mask is used to filter out unwanted higher diffraction orders attributed to the non-unity fill factor of the periodic array of SLM pixels.[17] The 4f relay is accompanied by demagnification which can be considered advantageous in this implementation, allowing for the pixel size to be easily modified. In principle, a reduction in exposure area is exactly compensated by an increased irradiance and thus reduced exposure time, for no net penalty to the overall throughput of the patterning process.

To demonstrate arbitrary patterning of liquid crystalline materials afforded by the ability to independently address the more than 10^6 pixels, a grayscale image (Fig. 1b) is recorded into an alignment cell and subsequently filled with liquid crystal monomer (Fig. 1). The surface is coated with a commercial photoalignment material (PAAD-22, BEAM Co) following procedures reported in ref. 13. The SLM plane is imaged onto a target surface, with 2 : 1 demagnification so that the pixel spacing in the target plane is nominally 16 μm. The approximately 1 cm^2 area was patterned by exposure with $\sim$100 mW cm^{-2} of 445 nm irradiation for 10 seconds. For comparison, preparing this pattern at this size scale using the raster method reported in ref. 13 would typically take more than 30 min. The method of ref. 18, using successive exposures modulated by a DMD, would also take approximately 30 min, based on reported parameters.

The effectiveness of polarization modulation of the SLM was characterized. With the SLM placed between a polarizer and analyzer, a grayscale signal is applied uniformly to all pixels and the transmitted intensity is measured as a function of analyzer angle. The result, shown in Fig. 2, confirms that the

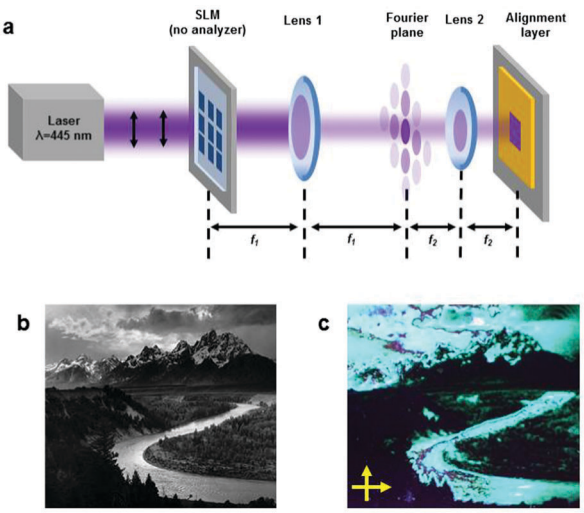

Fig. 1 (a) Projection lithography setup. The addressable SLM is imaged onto a photoalignment surface with magnification factor f_2/f_1. The amplitude mask in the Fourier plane eliminates unwanted higher diffraction orders. (b) Grayscale input to SLM. Image: Ansel Adams, "The Tetons and the Snake River." (c) Resulting pattern in 1 cm^2 area of a liquid crystal cell, viewed through crossed polarizers (15 μm cell thickness, filled with RM82).

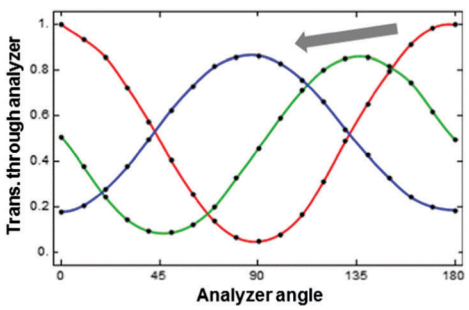

Fig. 2 By varying the 8-bit input (0–255) to an SLM pixel, the polarization of transmitted light can be rotated through as much as 90° while preserving low ellipticity. Here, the transmitted intensity through a rotating analyzer is plotted as a function of analyzer angle. The array of pixels is identically addressed, first with a signal level of 0 (red trace), then 153 (green trace), then 204 (blue trace). The peak of this curve, corresponding to the angle of linear polarization, is modulated through 90°.

incident s-polarization can be rotated through more than 90° while still maintaining a low ellipticity (<10%). Thus, not all linear polarization angles are accessible, although we will show below that the available range is still sufficient to implement many director profiles of interest including topological defects. Complete access to all possible polarization angles could be implemented *via* a more complicated double-pass layout, following ref. 19 or 20.

The size of the resolvable local volume elements (voxels) within a "programmed" LCN or LCE defines the lower bound for the scale of miniaturized mechanical elements prepared with these methods. To provide insight into the resolution limits, we make a number of best-case simplifying assumptions, following the analysis in ref. 21, and then compute the effect of Frank elastic energy minimization on voxel resolution. First, the Frank free elastic energy density of a director profile $\vec{n}$ is given by the familiar expression:

$$f = \frac{1}{2}K_1(\vec{\nabla}\cdot\vec{n})^2 + \frac{1}{2}K_2(\vec{n}\cdot\vec{\nabla}\times\vec{n})^2 + \frac{1}{2}K_3(\vec{n}\times\vec{\nabla}\times\vec{n})^2 \quad (1)$$

where the K_i are the elastic coefficients corresponding to bend, twist, and splay. Here we consider an alignment cell with two identically patterned planar alignment surfaces, although a similar analysis will hold for twisted nematic or hybrid alignment cells. In the case of zero pretilt, symmetry dictates that the director field $\vec{n}$ has a purely azimuthal orientation $\varphi(x,y,z)$, where the z-direction is normal to the alignment surfaces:

$$\vec{n}(x,y,z) = \begin{cases} \cos\varphi(x,y,z) \\ \sin\varphi(x,y,z) \\ 0 \end{cases} \quad (2)$$

In the approximation that all elastic coefficients are identical, the Frank energy density reduces simply to the Laplacian of $\varphi(x,y,z)$:

$$f = \frac{1}{2}K\left(\vec{\nabla}^2\varphi\right) \quad (3)$$

with fixed boundary conditions imposed by strong anchoring at the top and bottom alignment surfaces. Then, by the variational principle, the total elastic free energy $F = \int f\,\mathrm{d}v$ will be minimized when the 3D director profile satisfies $\mathrm{d}F/\mathrm{d}\varphi = 0$.

This condition is solved numerically for the first case of interest: the region near a border between two arbitrarily sharp alignment pixels of incompatible orientation (*e.g.* voxels in which the director is 90° offset from one another). As seen in Fig. 3(a), near the alignment surfaces the director reproduces this sharp transition, but farther from the surfaces, the director exhibits more gradual variation. Generalizing to three dimensions, consider a single alignment pixel surrounded on all sides by pixels of incompatible orientation. In this case, the director profile will maintain this pixel's templated alignment only within an hourglass-shaped volume, as shown in Fig. 3(b), rather than within a perfectly cuboidal voxel. This effectively limits the lateral feature resolution to the order of the cell thickness.

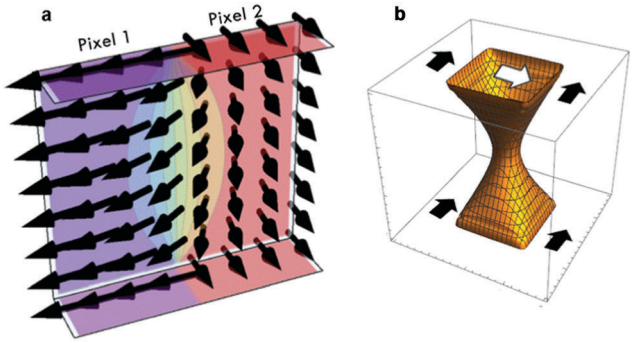

Fig. 3 (a) The calculated director field near the sharp boundary between two alignment pixels of incompatible orientation (here, 0° and 90°), showing a sharp transition enforced by strong anchoring at the top and bottom alignment surfaces, and a more gradual transition near the center of the cell. (b) An isolated alignment voxel, surrounded on all sides by a region of incompatible orientation. This voxel successfully templates the director field only within the hourglass-shaped volume. The thicker the cell, the more this hourglass deviates from a perfect cuboid. (The contour shown here indicates alignment to within 30% of the central pixel's orientation.)

The projection system described in Fig. 1 can experimentally validate this resolution limit. To this end, we record binary gratings at various spatial frequencies and measure the fringe visibility through crossed polarizers, taking the standard definition

$$V = \frac{I_{\max} - I_{\min}}{I_{\max} + I_{\min}} \quad (4)$$

We compare this with predictions based on the simple Frank elastic model described above, and find reasonable agreement at two different cell thicknesses (Fig. 4). In particular, the fringe visibility deteriorates when feature sizes are decreased to the

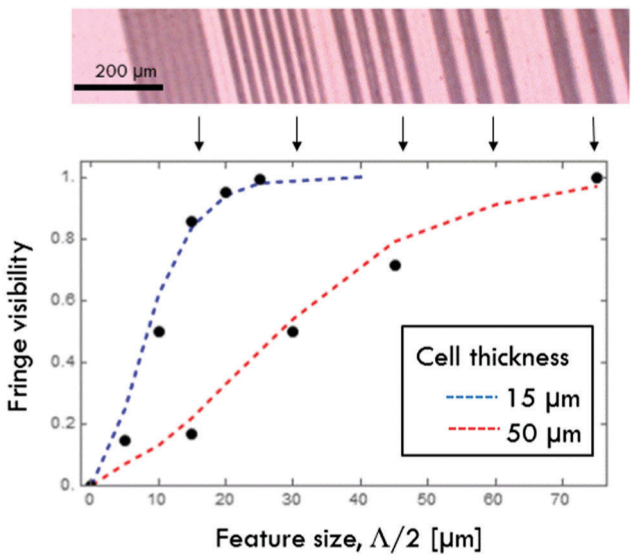

Fig. 4 Fringe visibility of a binary grating as a function of grating pitch. As predicted by a simple model (dashed lines) the measured fringe visibility (solid points) drops as the pitch approaches cell thickness. Two cases are shown: a 15 μm thick cell with 5 μm pixel spacing; and a 50 μm thick cell with 16 μm pixel spacing.

order of cell thickness. This is consistent with previous work[21] which calculated that the total Frank elastic energy penalty increases sharply as feature sizes approach the cell thickness. While these small features are also more prone to line defects, as seen in Fig. 1 above, it should be emphasized that orientational blurring is a distinct effect that is still present even in the ideal case of lowest-energy, defect-free alignment.

A direct visualization of this blurring effect is provided by imaging an ISO-standard resolution test pattern (Fig. 5a) onto an alignment surface. First, the alignment surface itself is visualized by examining a sub-micron spin-coated mesogen layer, following procedures described in ref. 13. This shows distinct, crisp patterning of the pixels at the surface (Fig. 5b). Next, identical photopatterning is performed on a 15 μm thick liquid crystal cell. Here the effect of orientational relaxation through the cell volume is clearly visible (Fig. 5c) as a smoothing of feature lines (*e.g.* the pixels/voxels).

Next, we demonstrate that this system can pattern director profiles of interest to realize complex 3D shape change. A profile with a topological defect of charge +1 forms a conical actuator.[22] Such +1 defects have previously been implemented with varying azimuthal director profiles,[13] but theoretical predictions suggest that a similar conical actuated shape can be realized from "segmented" defect profiles with only a few uniform regions of discretized orientation.[23] We pattern an LCE film with such a segmented defect profile, chosen so that all required polarization angles fall within the limited modulation range of the optical system. The resulting conical deformation forms a shape that is similar to that produced from a film with a continuously varying profile. In this way, we show here that +1 topological defects prepared from segmented or continuous director profiles exhibit nearly identical shape deformations.

Finally, we show that the voxel resolution limit inherent to these materials translates to a limit on the achievable size of actuating topological defects. Here, we reproduce the same +1 topological charge defect as before, but at a much smaller scale, so that the effective feature sizes approach the voxel resolution limit (on the order of the cell thickness). Fig. 7 shows the result of recording successively smaller isolated defect patterns into the same LCE formulation as above, with 15 μm cell thickness. For defect patterns down to 120 μm nominal diameter, the patterned director profile in the LCE is clearly visible under crossed polarizers and a well-defined cone actuates upward upon heating. Smaller defect patterns (Fig. 7c) do not retain the alignment due to the high Frank elastic energy penalties and yield a unresolvable pattern in the material that does not deform upon heating.

Materials and methods

Sample preparation

Alignment cells were self-prepared from glass slides (Colorado Concepts). Slides were spin-coated with photoalignment material, PAAD-22 (BEAM Co., 0.3 wt% in dimethylformamide). The cell gap was controlled by mixing 15 μm thick (except where otherwise specified) glass rod spacers into an optical adhesive.

Photopatterning was performed using a spatially filtered 445 nm DPSS laser and a twisted-nematic SLM (HoloEye LC2002). Cells were filled within 24 hours of photopatterning.

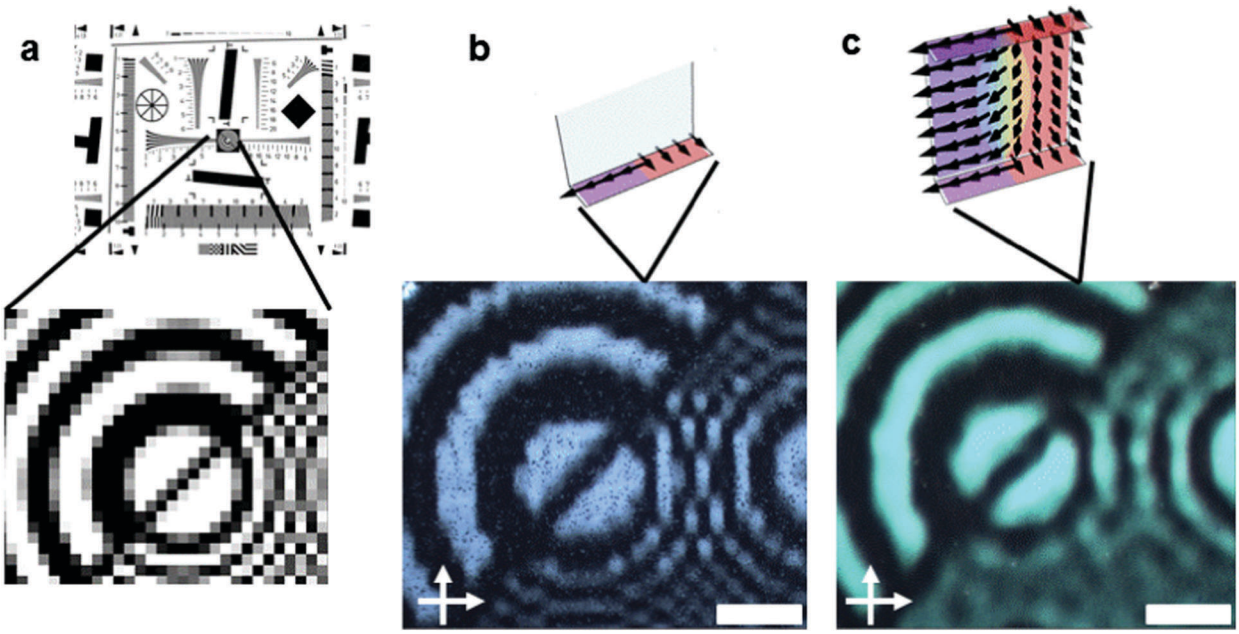

Fig. 5 Recorded test pattern to elucidate the voxel resolution limit. (a) ISO standard test pattern as displayed on the SLM. (b) Pattern as recorded at alignment surface, visualized with a spin-coated submicron layer of poly(RM257). Close agreement to the input pattern is apparent. (c) The resulting pattern templated through the thickness of a 15 μm cell filled with RM82. Pixel edges are smoothed out by the orientational relaxation of the material. Scale bars 100 μm.

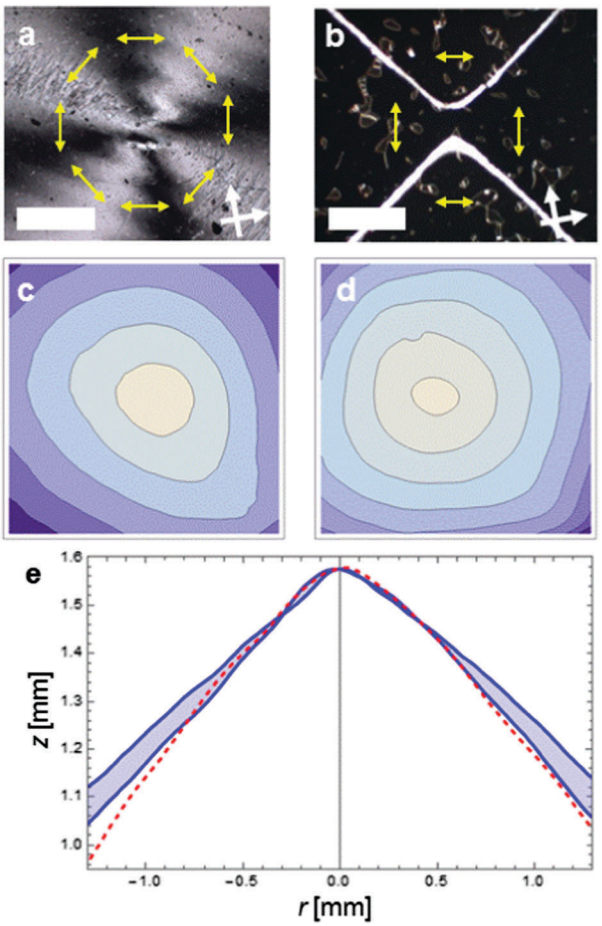

Fig. 6 Conical deformations arising from LCE films imprinted with director profiles described by +1 topological charge. Top: Polarized optical microscopy of LCE films showing (a) continuously varying profile, *via* raster photopatterning as in ref. 13 and (b) segmented defect with four uniform segments, *via* the SLM-based photopatterning described here. Scale bars: 100 μm. (c) and (d) The corresponding deformed shapes upon heating to 175 °C, as measured by optical 3D scanner. (e) Various radial profiles of the segmented defect (blue) show comparable shape and actuation distance to the continuous defect (red). Films are 50 μm thick; formulation is as described in ref. 24.

The polymerized samples examined in Fig. 4 and 5 were prepared using RM82 ((1,4-bis-[4-(6-acryloyloxyhexyloxy)benzoyloxy]-2-methylbenzene, Synthon)) doped with 1 wt% photoinitiator (Irgacure 651, BASF). Cells were filled at 135 °C, then cooled to 90 °C, where photoinitiated polymerization was undertaken with 50–80 mW cm^{-2} of 365 nm light (Exfo) for 3 min.

The freestanding films examined in Fig. 6 and 7 were prepared using a previously reported LCE formulation[24] consisting of a 0.5 : 1 : 1 molar ratio mixture of the following: RM82 (as above); 1,2-ethanedithiol (Sigma-Aldrich); and M05006 (2-methyl-1,4-phenylene bis(4-(3-(allyloxy)propoxy)benzoate, Synthon)). 1 wt% photoinitiator Irgacure 651 was added. Cells were filled at 100 °C, then cooled to 35 °C, whereupon photoinitiated polymerization was induced with 50–80 mW cm^{-2} of 365 nm light (Exfo) for 20 min.

Characterization

Quantitative measurements of the deformed shapes were obtained using a Keyence VR-3200 optical 3D scanner. Before scanning, samples were spray-coated with an opaque antireflective coating ("3D Scan Spray", Helling), since they would otherwise be optically transparent.

Conclusions

A rapid and scalable approach to photopatterning surface alignment is reported and employed to prepare voxelated LCNs and LCEs. The optical system requires only simple projection optics and a twisted-nematic SLM, which are available off-the-shelf or can be salvaged from an LCD projector.[25] In this way, this method is facile and easily accessible to non-specialists and may enable more rapid exploration of the opportunity space afforded by these materials.

As we detail hereto, surface alignment methods inherently have a voxel resolution limit defined not by the optical feature sizes, but rather by director variation throughout the depth of the cell. Experimental measurements of resolution are shown to be reasonably well explained by a simple model of orientational relaxation based on Frank free elastic energy. This effect imposes a minimum achievable size on actuating topological defects and other features of interest. It also acts to smooth out director discontinuities at the interfaces between nominally

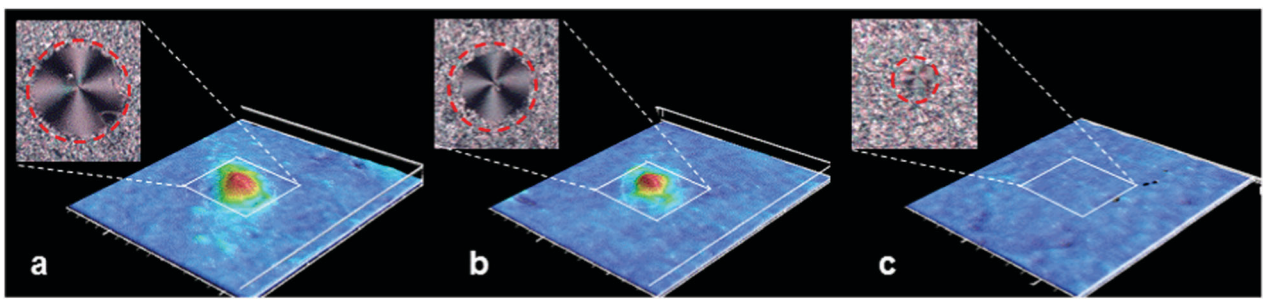

Fig. 7 Actuating defects realized at sub-mm scale, approaching the voxel resolution limit. Above: Polarizing optical microscope images of successively smaller patterned defects, with nominal diameters of (a) 160 μm, (b) (a) 120 μm, and (c) 80 μm (image width: 200 μm). Below: The corresponding deformations upon heating to 150 °C, as measured by 3D optical scanning. Note that for the smallest defect (c), Frank elastic energy penalties dominate, and the LCE is mostly polydomain and exhibits no deformation. LCE film is 15 μm thick; material formulation is as described in ref. 24.

incompatible domains; thus, it is relevant to efforts to optimize topology for designed curvatures or hinge angles.

Acknowledgements

The authors acknowledge funding from the Air Force Office of Scientific Research and the Materials and Manufacturing Directorate of the Air Force Research Laboratory.

Notes and references

1 T. H. Ware, J. S. Biggins, A. F. Shick, M. Warner and T. J. White, Localized soft elasticity in liquid crystal elastomers, *Nat. Commun.*, 2016, **7**, 10781.
2 S. V. Serak, D. E. Roberts, J.-Y. Hwang, S. R. Nersisyan, N. V. Tabiryan, T. J. Bunning, D. M. Steeves and B. R. Kimball, Diffractive waveplate arrays [Invited], *JOSA B*, 2017, **34**, B56.
3 J. Küpfer and H. Finkelmann, Nematic liquid single crystal elastomers, *Makromol. Chem., Rapid Commun.*, 1991, **12**, 717.
4 C. E. Hoyle, T. Watanabe and J. B. Whitehead, Anisotropic network formation by photopolymerization of liquid crystal monomers in a low magnetic field, *Macromolecules*, 1994, **27**, 6581.
5 D. L. Thomsen, P. Keller, J. Naciri, R. Pink, H. Jeon, D. Shenoy and B. R. Ratna, Liquid crystal elastomers with mechanical properties of a muscle, *Macromolecules*, 2001, **34**, 5868.
6 A. J. Pidduck, S. D. Haslam, G. P. Bryan-Brown, R. Bannister and I. D. Kitely, Control of liquid crystal alignment by polyimide surface modification using atomic force microscopy, *Appl. Phys. Lett.*, 1997, **71**, 2907.
7 T. Seki, S. Nagano and M. Hara, Versatility of photoalignment techniques: from nematics to a wide range of functional materials, *Polymer*, 2013, **54**, 6053.
8 O. Yaroshchuk and Y. Reznikov, Photoalignment of liquid crystals: basics and current trends, *J. Mater. Chem.*, 2012, **22**, 286.
9 W. M. Gibbons, P. J. Shannon, S.-T. Sun and B. J. Swetlin, Surface-mediated alignment of nematic liquid crystals with polarized laser light, *Nature*, 1991, **351**, 49.
10 M. McConney, A. Martinez, V. Tondiglia, K. Lee, D. Langley, I. Smalyukh and T. J. White, Topography from topology: photoinduced surface features generated in liquid crystal polymer networks, *Adv. Mater.*, 2013, **25**, 5880.
11 G. P. Crawford, J. N. Eakin, M. D. Radcliffe, A. Callan-Jones and R. A. Pelcovits, Liquid-crystal diffraction gratings using polarization holography alignment techniques, *J. Appl. Phys.*, 2005, **98**, 123102.
12 Y. Guo, M. Jiang, C. Peng, K. Sun, O. Yaroshchuk, O. Lavrentovich and Q.-H. Wei, High-Resolution and High-Throughput Plasmonic Photopatterning of Complex Molecular Orientations in Liquid Crystals, *Adv. Mater.*, 2016, **28**, 2352.
13 T. H. Ware, M. E. McConney, J. J. Wie, V. P. Tondiglia and T. J. White, Voxelated liquid crystal elastomers, *Science*, 2015, **347**, 982.
14 M. N. Miskiewicz and M. J. Escuti, Direct-writing of complex liquid crystal patterns, *Opt. Exp.*, 2014, **22**, 12691.
15 Y. Xia, G. Cedillo-Servin, R. D. Kamien and S. Yang, Guided Folding of Nematic Liquid Crystal Elastomer Sheers into 3D *via* Patterned 1D Microchannels, *Adv. Mater.*, 2016, **28**, 9637.
16 A. Ogiwara and T. Hirokari, Formation of anisotropic diffraction gratings in a polymer-dispersed liquid crystal by polarization modulation using a spatial light modulator, *Appl. Opt.*, 2008, **47**, 3015.
17 M. Agour, E. Kolenovic, C. Falldorf and C. von Kopylow, Suppression of higher diffraction orders and intensity improvement of optically reconstructed holograms from a spatial light modulator, *J. Opt. A: Pure Appl. Opt.*, 2009, **11**, 105405.
18 C. Culbreath, N. Glazar and H. Yokoyama, Note: Automated maskless micro-multidomain photoalignment, *Rev. Sci. Instrum.*, 2011, **82**, 126107.
19 T. K. Ewing, S. V. King, H. M. Masterson, N. Gonzales and D. Elshof, Development of a polarization hyperspectral image projector, in *SPIE Defense, Security, and Sensing*, 2012.
20 I. Moreno, J. A. Davis, T. M. Hernandez, D. M. Cottrell and D. Sand, Complete polarization control of light from a liquid crystal spatial light modulator, *Opt. Exp.*, 2012, **20**, 364.
21 K. Kawai, T. Sasaki, K. Noda, N. Kawatsuki and H. Ono, Simple fabrication of liquid crystalline grating cells with homogeneous and twisted nematic structures and effects of orientational relaxation on diffraction properties, *Appl. Opt.*, 2014, **53**, 3679.
22 C. Mostajeran, M. Warner, T. H. Ware and T. J. White, Encoding Gaussian curvature in glassy and elastomeric liquid crystal solids, *Proc. R. Soc. A*, 2016, **472**, 20160112.
23 C. D. Modes and M. Warner, Blueprinting nematic glass: Systematically constructing and combining active points of curvature for emergent morphology, *Phys. Rev. E: Stat., Nonlinear, Soft Matter Phys.*, 2011, **84**, 021711.
24 T. H. Ware, Z. P. Perry, C. M. Middleton, S. T. Iacono and T. J. White, Programmable liquid crystal elastomers prepared by thiol-ene photopolymerization, *ACS Macro Lett.*, 2015, **4**, 942.
25 D. Huang, H. Timmers, A. Roberts, N. Shivaram and A. S. Sandhu, A low-cost spatial light modulator for use in undergraduate and graduate optics labs, *Am. J. Phys.*, 2012, **80**, 211.

